LBNL-42654

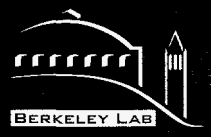

ERNEST ORLANDO LAWRENCE
BERKELEY NATIONAL LABORATORY

Magnetic Fields of AM Band Radio Broadcast Signals at the Richmond Field Station

William Frangos and Alex Becker

Earth Sciences Division

December 1998

LBNL-42654

Magnetic Fields of AM Band Radio Broadcast Signals at the Richmond Field Station

William Frangos and Alex Becker
Earth Sciences Division
Ernest Orlando Lawrence Berkeley National Laboratory
University of California
Berkeley, California 94720

December 1998

This work was carried out under U.S. Department of Energy Contract DE-AC03-76SF-00098. Funding was provided by the U.S. Department of Energy, the Environmental Management Sciences Program, as EMSP Project No. 60328.

Magnetic Fields of AM Band Radio Broadcast Signals at the Richmond Field Station

William Frangos and Alex Becker
Earth Sciences Division

Introduction

Non-invasive sensing of the shallow subsurface is necessary for detection and delineation of buried hazardous wastes, monitoring of the condition of clay containment caps, and a variety of other purposes. Electromagnetic methods have proven to be effective in environmental site characterization where there is a need for increased resolution in subsurface characterization. Two considerations strongly suggest the use of frequencies between 100 kHz and 100 MHz for such applications: 1) the induction response of many targets is small due to small size, and 2) a need to determine both the electrical conductivity and dielectric permittivity which are related to chemistry and hydrology. Modeling and physical parameter studies confirm that measurements at frequencies between 1 and 100 MHz can resolve variations in subsurface conductivity and permittivity. To provide the necessary technology for shallow subsurface investigations, we propose to exploit the concept of electromagnetic impedance, the ratio of orthogonal horizontal electric and magnetic fields.

Prior to assembling the equipment for measuring surface impedance using a controlled, local source it was felt prudent to measure the surface impedance of geological materials at the University of California at Berkeley's Richmond Field Station (RFS) using ambient energy in the broadcast band. As a first step toward this intermediate goal, we have examined and characterized local AM band radio signals in terms of both signal strength and polarization of the magnetic component as received at RFS. In addition, we have established the viability of a commercial radio-frequency magnetic sensor.

Field Determination from Three-component Measurements

Observation of three complex spatial components of the magnetic field allows its complete. The field is, in general, elliptically polarized, with the plane of the ellipse inclined in space. Full specification requires identification of the plane of polarization and the ellipse parameters within that plane.

The characterization of a polarization ellipse for a plane wave with arbitrary in-plane orthogonal components and their phase difference has been well described by Born and Wolf (*c.f.*, 1970, p. 25-27), with particular reference to optics. Morgan and Evans (1951) discuss ellipses of polarization in three dimensions, showing geometrically that any monochromatic wave characterized by three mutually orthogonal components may be described as a planar ellipse. Stutzman (1993) provides a comprehensive discussion of plane polarization in electromagnetic systems, while Booker, *et al.* (1951) consider elliptical polarization with respect to antennas. Deschamps and Mast (1973) extend the work of Booker, *et al.* (1951) to include partially polarized fields, *i.e.,* those having both a polarized and a random component. Smith and Ward (1974), the appendix of McNeill and Labson (1990), Bak, *et al.* (1993), and Thomas (1996) provide a geophysical approach. It must be noted that the various workers cited above, as others who have considered the problem, employ a variety of different conventions. In particular, the axial ratio, or ellipticity is defined as

$$\varepsilon = \frac{Minor\ axis}{Major\ axis}, \text{ such that } 0 \le \varepsilon \le 1, \qquad (1)$$

by the majority of the workers, including the geophysical papers, while Stutzman (1993), the current IEEE standard (1983), and contemporary antenna engineers use the reciprocal, so that $1 \le \varepsilon \le \infty$. Other discrepancies are noted in the definition of rotational sense, direction of viewing the wave, and whether the "ellipticity" is the ratio of ellipse axes or the arctangent thereof (also called "ellipticity angle"). In addition, as Stutzman (1993) notes, there are two different sets of ellipse parameters in common use: tilt angle and ellipticity, or the amplitude ratio of two orthogonal components and the phase angle between them.

We shall take as ellipticity the axial ratio defined in Eqn. (1) above, and define tilt angle, θ, following Smith and Ward (1974), as

$$\tan 2\theta = \frac{2R\cos\delta}{1-R^2} \tag{2}$$

where $R = |H_x| / |H_y|$ and

δ is the phase angle between the two (observed) orthogonal components, from which it follows that

$$\begin{aligned} \varepsilon &= \frac{H_x H_y \sin\delta}{(H_x \sin\theta\cos\delta + H_y\cos\theta)^2 + (H_x\sin\theta\sin\delta)^2} \\ &= \frac{2R\sin\delta}{(1+R^2)-(1-R^2)\sec 2\theta} \end{aligned} \tag{3}$$

The magnetic field generated by a vertical electric dipole exhibits linear polarization and remains so indefinitely in free space or over a homogeneous or layered earth. In the presence of 2- or 3-D inhomogeneities, however, secondary fields may render the polarization elliptical. The total field, being the sum of both the primary field and the secondary fields induced in the inhomogeneities, may be deflected from its free space direction. This concept is exploited as the "induction arrow" in geomagnetic depth sounding (Gregori and Lanzerotti, 1980, and Parkinson, 1982).

The challenge is to describe the arbitrarily inclined plane and the ellipse parameters from measurements of three mutually spatially orthogonal components of temporally complex phasors. It is important to maintain the distinction between spatial and temporal angles in the following. The notion, described in detail below, is to use one of the observed components as a phase reference for the three spatial components. The plane of polarization, within which the ellipse lies, may be determined by extracting the two temporally orthogonal resultant vectors, Re and Im, from the original three observations; the normal to this plane may be determined by the cross product of the

vectors. Further, two spatially orthogonal (but not temporally orthogonal) components within this plane may be calculated from the two vectors and the angle between them. Standard methods of Born and Wolf (1970) may then be applied to the spatially orthogonal vectors and the phase (temporal) angle between them to determine the ellipse parameters within the plane.

A total of five parameters are required to characterize the ellipse completely. We use the direction cosines of the unit normal to describe the attitude of the plane, and ellipticity and tilt for the axial ratio and attitude of the ellipse within its plane. The coordinate system is aligned with the x-axis extending from the source to the receiver. Thus, in the usual conditions, the x-axis is horizontal and in the line-of-sight, the z-axis is vertical and positive upwards and the y-axis is horizontal and positive to form a right-handed coordinate system.

In view of the wide range of conventions commonly employed to describe the polarization ellipse, a listing of some of the other possibilities is in order. The Poincare parameters are often used by antenna engineers as an alternative to the ellipse parameters, tilt and ellipticity; the Poincare parameters are defined as twice the arctangent of the ellipticity (*i.e.*, the axial ratio) and twice the tilt angle. The Poincare parameters are often plotted as points on the surface of a sphere, using the double ellipticity angle as latitude and the double tilt angle as longitude. Different projections of the Poincare sphere onto a plane form the Carter and Smith charts (Theocaris, 1979). One intuitive alternative for characterizing the attitude of the plane is the use of Euler angles, describing the re-orientation of a plane as three rotations, using the pilot's terms of roll, pitch, and yaw. Conceptually, this definition corresponds to the attitude of an airplane flying away from the origin along the positive x axis, with the z axis pointed upward. Other expressions that are used in important literature references include the Stokes parameters (Kraus, 1982, and Born and Wolf, 1970), the complex vector representation (Kales *in* Booker *et al.*, 1951 and IEEE Standard 145-1983), and the polarization ratio (Rumsey *in* Booker, *et al.*, 1951, and Beckman, 1968). Alternative descriptors for the attitude of the polarization plane include the Wulff net and stereonet familiar from structural geology, and the

rotation of the normal to the polarization plane in terms of rotation matrices, Euler parameters (a more computationally facile form of Euler angles), and quaternions.

Consider three spatially orthogonal components of a time varying magnetic field,

$$\begin{aligned} H_x &= H_x^0 \sin(\omega t + \phi_x) \\ H_y &= H_y^0 \sin(\omega t + \phi_y) \\ H_z &= H_z^0 \sin(\omega t + \phi_z) \end{aligned} \tag{4}$$

and take H_y as the reference, as is appropriate for observation of the signal due to a vertical electric dipole at a point displaced along the *x*-axis, such that $\phi_y = 0$ and henceforth

$$|H_x| = {|H_x|}/{|H_y|}, \quad |H_y| = 1.0, \quad \text{and} \quad |H_z| = {|H_z|}/{|H_y|}. \tag{5}$$

The magnitudes of the total real and imaginary field vectors then are

$$\begin{aligned} |\mathrm{Re}| &= \sqrt{\mathrm{Re}_x^2 + 1 + \mathrm{Re}_z^2} \\ |\mathrm{Im}| &= \sqrt{\mathrm{Im}_x^2 + 0 + \mathrm{Im}_z^2} \end{aligned} \tag{6}$$

where $\mathrm{Re}_x = |H_x|\cos\phi_x$, $\mathrm{Re}_z = |H_z|\cos\phi_z$, $\mathrm{Im}_x = |H_x|\sin\phi_x$, $\mathrm{Im}_z = |H_z|\sin\phi_z$

Note that the Im vector is completely within the x-z plane, a consequence of the choice of H_y as the reference component. Let the angles between the coordinate axes and the Re and Im vectors be designated α_{Re}, β_{Re}, and γ_{Re} and α_{Im}, β_{Im}, and γ_{Im}, respectively. Then the direction cosines for each vector are

$$\begin{aligned} \cos\alpha_{\mathrm{Re}} &= {\mathrm{Re}_x}/{|\mathrm{Re}|} \\ \cos\beta_{\mathrm{Re}} &= {\mathrm{Re}_y}/{|\mathrm{Re}|} = {H_y}/{|\mathrm{Re}|} = {1}/{|\mathrm{Re}|} \\ \cos\gamma_{\mathrm{Re}} &= {\mathrm{Re}_z}/{|\mathrm{Re}|} \\ \cos\alpha_{\mathrm{Im}} &= {\mathrm{Im}_x}/{|\mathrm{Im}|} \\ \cos\beta_{\mathrm{Im}} &= 0 \\ \cos\gamma_{\mathrm{Im}} &= {\mathrm{Im}_z}/{|\mathrm{Im}|} \end{aligned} \tag{7}$$

and the spatial angle between the resultant real and imaginary vectors, ψ, can be found from (*e.g.*, Burrington, 1933, p.34)

$$\cos\psi = \cos\alpha_{\mathrm{Re}}\cos\alpha_{\mathrm{Im}} + \cos\beta_{\mathrm{Re}}\cos\beta_{\mathrm{Im}} + \cos\gamma_{\mathrm{Re}}\cos\gamma_{\mathrm{Im}} \tag{8}$$

Now the normal to the plane of polarization, and thus its attitude, may be found by taking the cross product of the two vectors

$$\vec{n} = \vec{\mathrm{Re}} \times \vec{\mathrm{Im}} = \begin{vmatrix} \hat{x} & \hat{y} & \hat{z} \\ \mathrm{Re}_x & \mathrm{Re}_y & \mathrm{Re}_z \\ \mathrm{Im}_x & \mathrm{Im}_y & \mathrm{Im}_z \end{vmatrix} \tag{9}$$

In the particular case of using the amplitude-normalized y-component as the reference vector per Eq. (5), we note that

$$\vec{n} = \begin{vmatrix} \hat{x} & \hat{y} & \hat{z} \\ \mathrm{Re}_x & 1 & \mathrm{Re}_z \\ \mathrm{Im}_x & 0 & \mathrm{Im}_z \end{vmatrix} = \mathrm{Im}_z\hat{x} + (\mathrm{Re}_z\,\mathrm{Im}_x - \mathrm{Re}_x\,\mathrm{Im}_z)\hat{y} - \mathrm{Im}_x\hat{z} \tag{10}$$

so that the attitude in the x-z plane depends solely on the imaginary x- and z-components.

Further, it is often convenient to deal with a *unit* normal vector to normalize the component amplitudes. To accomplish this, we may divide each of the components immediately above by the magnitude of the normal vector, getting

$$\hat{n} = \vec{n} \Big/ |n| \tag{11}$$

The in-plane spatially orthogonal components may be composed, for example, by projecting the Im vector onto the Re vector to form a temporally complex "Direction of Real" (DOR) vector,

$$DOR = \mathrm{Re} + i\,\mathrm{Im}\cos\psi = \sqrt{\mathrm{Re}^2 + (\mathrm{Im}\cos\psi)^2} \qquad \angle\tan^{-1}\left(\mathrm{Im}\cos\psi / \mathrm{Re}\right) \qquad (12)$$

and a purely imaginary "Normal to Real" (NTR) vector,

$$NTR = i\,\mathrm{Im}\sin\psi \qquad (13)$$

The phase between these two components is then

$$\delta = \pi/2 - \tan^{-1}\left(\mathrm{Im}\cos\psi / \mathrm{Re}\right) \qquad (14)$$

which may be inserted into the standard tilt and ellipticity expressions, Eqns. (2) and (3) above, to determine the ellipse parameters within the plane of polarization,

$$\textit{Tilt}, \quad \theta = \frac{1}{2}\tan^{-1}\left(\pm 2\frac{DOR/NTR\,\cos\delta}{1-\left(DOR/NTR\right)^2}\right) \qquad (15)$$

$$\textit{Ellipticity}, \quad \varepsilon = \frac{DOR\cdot NTR\cdot\sin\delta}{\left(DOR\sin\theta\,\cos\delta + NTR\cos\theta\right)^2 + \left(DOR\sin\theta\sin\delta\right)^2} \qquad (16)$$

Experimental Procedure

Two EMCO Model 6507 loop antennas, serial numbers 9012-1257 and 9010-1240, referred to hereinafter as "A" and "B", respectively, were borrowed from DOE's Grand Junction (Colorado) office. These devices are represented by the manufacturer to be useful between 1 kHz and 30 MHz; they are used commercially for testing antenna radiation patterns and monitoring broadcast coverage. Appendix 1 is a copy of the individual calibration data for one of the antennas. The basic design is of a single

circular turn of wire about 30 cm. in diameter, electrically shielded within a split tube, and terminated into an integral high-impedance amplifier. The output impedance of the device is 50 Ω, through a female BNC connector mounted on the metallic base which houses the amplifier and internal batteries.

The measuring instrument throughout this work was a Hewlett Packard HP89410A Vector Signal Analyzer. This device provides two channels of digital data acquisition and analysis at frequencies between 0.01 Hz and 10 MHz, as well as providing a reference signal of variable amplitude and waveform. Observed data may be recorded directly onto a standard 3½ inch floppy diskette.

Antenna Calibration

Fixed-source Calibrations

A large cylindrical solenoid was used as a known magnetic field source. The solenoid is too small to accommodate the EMCO coil inside, so measurements had to be made external to the solenoid. Two systems of measurement were used: 1) the external field was calculated and compared to the field reported by the EMCO coil using the manufacturer's antenna factors, and 2) a high-frequency EMI model BF-6 coil, with fairly flat response up to 100 kHz, was used as a transfer standard. In the latter procedure, the BF-6 was placed inside the solenoid and calibrated over its useful range, noting that the results agreed well with the manufacturer's calibration. The BF-6 was then placed outside the solenoid, along the axis, and another set of measurements taken. The EMCO coil was then positioned at the same place, and its output observed in the empirically calibrated axial field of the solenoid. This empirical procedure was undertaken out of concern that nearby conductive and ferrous objects might perturb the solenoid field from its theoretical value.

The magnetic field inside a long solenoid is given as:

$$H_{inside} = nI \tag{17}$$

where I is the current flowing in the solenoid, and

n is the number of turns per meter of the solenoid.

The solenoid is 164 inches long and has 83 turns, or exactly ½ turn per inch, equivalent to 19.7 turns per meter.

It is important to monitor the current in the solenoid with a low-valued resistor located near the solenoid input to avoid capacitive losses and to use low impedance measuring circuitry in order to avoid spurious capacitive pickup on the leads. While the EMCO antennas are designed for a 50 ohm input impedance, the BF-6 coils are intended to be matched to an infinite impedance measuring system. The HP89410A provides a random noise output, useful for defining transfer functions. There is a trade-off in setting the HP89410A output level and the bandwidth of the random noise measurement. The amplitude of the BF-6 output exceeds the linear range of the HP89410A input for HP89410A output levels that yield erratic spectra near the lower and upper frequency limits. Pragmatically, better averaging and smoother spectra result when the random noise spectrum is limited to about two decades and the BF-6 output is attenuated by a factor of about 20. A Tektronix optical link was employed as an attenuator, after careful full spectrum calibration, also affording an impedance matching function by providing a high input impedance for the BF-6 and a low output impedance for transmitting the signal to the HP89410A. Empirical corrections were made for coax cable losses, including the effects of the reactive solenoid. Figure 1 shows schematic diagrams for the measuring setups.

Using three scans of a two-decade bandwidth and 1601 frequencies for each scan, reasonably smooth calibration spectra may be found over the range 1.0 Hz to 1 MHz. Figure 2 shows the calibration sensitivity and phase spectra for the BF-6 in the solenoid, a total of 4801 frequencies. Note the interfering signals from broadcast stations at the high end and from the power grid at 60 and 180 Hz.

External Field of a Solenoid

The field on the axis outside the solenoid may be calculated as follows. The magnetic field on the axis of a single loop of current, I, and radius, a, at a distance, z, is (*e.g.*, Halliday and Resnick, 1960, p.770)

$$H_{axis} = \frac{Ia^2}{2(a^2 + z^2)^{3/2}} \tag{18}$$

The solenoid may be treated as a continuous length, L, of such loops having a current distribution *nI* Amps/m, and integration over them yields the on-axis field at an exterior point, distant Z from the end.

$$\begin{aligned} H_{Solenoid-axis} &= \int_{near-end}^{far-end} H_{axis}\, dz = \frac{nIa^2}{2} \int_Z^{Z+L} \frac{dz}{(a^2 + z^2)^{3/2}} = \frac{nI}{2} \frac{z}{\sqrt{z^2 + a^2}} \Big|_Z^{Z+L} \\ &= \frac{nI}{2} \left\{ \frac{Z+L}{\sqrt{(Z+L)^2 + a^2}} - \frac{Z}{\sqrt{Z^2 + a^2}} \right\} \end{aligned} \tag{19}$$

The field strength outside the solenoid proved to be too weak for accurate measurements using the HP89410A source as a random noise generator. Accordingly, the signal source was used in sine wave mode and spot readings were taken at various frequencies between 1 kHz and 1 MHz and at a distance of 5 m from the end of the solenoid. Table I presents the results of this experiment. The BF-6 coil, acting as a transfer standard, serves to verify the calculated field strength outside the solenoid. The EMCO, using interpolated values of the manufacturer's supplied calibration information, appears to yield the calculated field within a few percent except at the lowest frequency, where noise overrides the antenna's lack of sensitivity, and at the highest, where the solenoid resonances complicate matters. The manufacturer's calibration data seem well justified.

Table I: Measured and Calculated Axial Fields External to the Solenoid

	Observed Fields		Calculated Fields			
	EMCO	BF-6	EMCO	BF-6	Ratio, Obs/Calc'd:	
	uA/m	uA/m	uA/m	uA/m	EMCO	BF-6
Freq, Hz						
1.0E+03	48.3	40.7	35.67	35.64	1.35	1.14
2.0E+03	32.7	33.7	35.50	35.45	0.92	0.95
4.0E+03	33.3	31.6	35.29	35.26	0.94	0.90
7.0E+03	33.7	32.2	34.97	34.94	0.96	0.92
1.0E+04	33.5	31.6	34.55	34.52	0.97	0.92
2.0E+04	31.7	26.9	32.53	32.50	0.97	0.83
4.0E+04	27.1	22.2	27.13	27.12	1.00	0.82
7.0E+04	20.4	18.6	20.11	20.10	1.02	0.92
1.0E+05	16.8	13.7	15.47	15.46	1.09	0.88
2.0E+05	8.9	8.3	8.39	8.39	1.06	0.99
4.0E+05	4.6	11.2	4.20	13.32	1.10	0.84
7.0E+05	2.2	15.8	2.18	21.90	1.01	0.72
1.0E+06	0.9	12.1	1.19	11.96	0.79	1.01

Figure 3 shows the interpolated manufacturer's calibration data over the usable spectrum as calibration factor; in Appendix I appears the same information in the forms of sensitivity, antenna factor, and effective area for convenience.

As a further test, it was desired to verify that the EMCO antennas exhibit the same sensitivity to a vertical magnetic field as to the horizontal fields for which they are designed and for which they are normally used. To effect this evaluation, we used a smaller solenoid that could be conveniently positioned on end to generate a vertical magnetic field. Field values read in the horizontal and vertical poses agreed within about 5%, consistent with the spacing achieved in a mechanically unstable set-up.

Angular Sensitivity

As a general test of the antenna behavior, and to verify its appropriateness for measuring the vector components of the magnetic fields, the directional response of the antennas was measured. This was done by observing the horizontal field while rotating the antenna in small increments. An electric field monopole was used as the amplitude standard for this work (one of the magnetic dipole batteries had become weak and would not last through the time it took to complete a data set). A pattern of angular lines was drawn on a piece of stiff cardboard using a protractor, and the cardboard aligned with geographic north using a Brunton compass. The antenna was then aligned by eye with the inscribed lines. Overall alignment accuracy was estimated to be approximately ±2°. Two transmitters were used for this exercise, KNEW at 910 kHz and the one at 55.5 kHz. Figure 4 presents the EMCO loop antenna output normalized by the E_z signal and multiplied by an appropriate scaling constant at a variety of angular positions. Also shown is the angular radiation pattern of an ideal dipole, given by the expression

$$\begin{Bmatrix} x \\ y \end{Bmatrix} = \frac{\sqrt{4\cos^2\theta + \sin^2\theta - 1}}{\sqrt{3}} \begin{Bmatrix} \cos\theta \\ \sin\theta \end{Bmatrix} \tag{20}$$

An alternate test of the directional sensitivity was made by determining the direction of the major axis of the apparent polarization ellipse in the horizontal plane and comparing it with the expected direction based on the known transmitter location. In order to accomplish this, one need only measure orthogonal horizontal components in known directions and apply the ellipse-tilt equation, Eqn. (2), to the two horizontal components. Figure 5 presents the bearings of each of the 16 selected AM radio stations, in degrees from north, plotted in a spectral format. Also shown are the true directions as measured on a map and the differences between the estimated and true directions. The agreement is excellent for all stations except KSFO at 560 kHz. Averaging a large

number of data scans was necessary for this determination; these determinations are based on averages of 150 scans.

The possibility was considered that the EMCO antenna might have a directional dependence in the vertical mode due to currents induced in the rectangular base by the much stronger horizontal magnetic component. One antenna was positioned with its axis vertical and measured the field at different rotational orientations, using the other as a reference observing the maximum horizontal field at 910 kHz. A carpenter's level and tapered shims served to position the vertical sensor. The data are relatively noisy, due to the fact that the vertical field is weak, but no systematic response differences were noted.

Noise Measurements

The HP89410A provides the ability to report the coherence between two signals. Exploiting this feature, we can determine the noise level of the EMCO sensors following a method described by Nichols, *et al.*, (1988). The notion is to measure the same signal simultaneously with two sensors and note the coherence between the two time series. Any differences may be considered noise, thus

$$NoisePower = \frac{Signal^2 \cdot (1 - Coh)}{Freq}$$

$$or, \qquad (21)$$

$$Noise = \sqrt{NoisePower}$$

Figure 6 shows the observed noise spectrum between 1 kHz, the low end of the EMCO response, and 10 MHz, the maximum frequency of the HP89410A, in units of equivalent (Amps/m) / √Hz. The EMCO antenna noise dominates the lower frequency range, showing characteristic $1/f$ noise.

Proximity Tests

The possibility of interaction between closely positioned coils is another concern requiring investigation. Each loop and its attendant electronics and cables represent a potential field disruption. A series of ratios between the two coils' outputs were read, all of which were within a few percent of unity.

Results

Ambient Field

Observations of the ambient field were performed at the University of California Richmond Field Station, located near the eastern shore of San Francisco Bay at approximately 122° 20'W, 38° 55'N or 558,000E, 4,185,000N, UTM zone 10. Many of the data shown here were recorded on 23 September 1998. There are numerous broadcast, navigation, and military transmitters in the area, operating at frequencies between 55.5 kHz and 1.64 MHz. These can be used for developing a sensor system.

The dominant signals are the AM broadcast stations. The strongest signal is KNEW at 910 kHz, whose 5,000-watt transmitter is located about 1.9 km from the RFS site. Fourteen of the remaining 15 stations are situated generally south of RFS in San Francisco, Berkeley, Oakland, and the South Bay. One station, KCBS at 740 kHz, lies north of RFS in the town of Novato. The stations are scattered about an azimuthal range of about 50° as viewed from RFS. While the total radiated power of each AM station is constant with time (except for day-night shifts for some), the effects of modulation and of variations along the transmission path cause the amplitude at the receiver to vary by as much as 10 dB over a span of a few seconds to several minutes. Accordingly, it is necessary to make all observations with respect to a reference sensor. Table II summarizes the AM radio stations used as signal sources for most of this work.

The AM stations occupy a 20 kHz bandwidth, into which their modulation sidebands are fit. Figure 7 shows in detail a typical averaged spectrum for KNEW.

Table II: Broadcast AM Transmitters

Freq, kHz	Call Sign	Transmitter Location	Power, kW	Bearing from RFS	Distance, km	Magnetic Field, A/m
560	KSFO	South SF	5	S10°W	28	1.304e-04
610	KFRC	Ashby Ave, Berkeley	5	S22°E	7.2	2.788e-04
680	KNBR	Redwood City	50	S15°E	45	2.574e-04
740	KCBS	Novato	50	N34°W	26.5	5.361e-04
810	KGO	East end Dumbarton Bridge	50	S27°E	47	3.447e-04
910	KNEW	racetrack	5	S18°E	1.9	1.050e-03
960	KABL	Bay Bridge toll plaza	5	S10°E	9.2	2.465e-04
1010	KIQI	Bay Bridge toll plaza	10	S10°E	9.2	1.435e-04
1050	KTCT	Hayward	50	S28°E	32.8	8.501e-05
1100	KFAX	East end San Mateo Bridge	50	S26°E	37	2.304e-04
1220	KDTA	Palo Alto		S22°E	53	3.575e-05
1260	KOIT	Candlestick Hill, SF	5	S12°W	22	9.107e-05
1310	KDIA	Bay Bridge toll plaza	5	S10°E	9.2	8.148e-05
1400	KVTO	Ashby Ave., Berkeley	1	S22°E	7.2	1.316e-04
1450	KEST	Pier 70, SF	1	S14°W	17	4.370e-05
1550	KYCY	West end San Mateo Bridge	10	S 9°E	38	8.302e-05

Two other transmitters were found to be of use, one at 55.5 kHz and the other at 100 kHz. Details of these transmitters are not known; the 100 kHz source has a

particularly intricate modulation pattern and broad, complicated sidebands. Several other transmitters were noted at various times, but were not consistently on the air, and were not used. Signals were not consistently recognizable from such standard broadcast stations as WWV at 2.5, 5, and 10 MHz and medium-wave broadcasts; the EMCO noise level obscures these sources.

Amplitude Observations

Observed three-component spectra over the useful range of the EMCO coils, between 1 kHz and 10 MHz, are presented as Figures 8, 9, and 10. For improved spectral resolution, the data were taken in two adjacent frequency bands, 1 kHz – 100 kHz and 100 kHz – 10 MHz. Furthermore, having only two sensors and variable sources (*e.g.*, the transmission path and modulation variations of the AM stations), it was necessary to measure the components in separate runs with a standard reference component and normalize the observed spectral amplitudes in order to compare relative component strengths. With deference to the strongest and most reliable of the observed signals, the standard to which other data were normalized was the E-W component of the first data run, the "Master" record. Calibration factors, *CF*, interpolated for each frequency were applied to the data. Each datum in Figures 8, 9, and 10 is calculated as

$$H_{component} = V_{observed} * CF * \frac{V_{Mast}}{V_{Ref}} \qquad (22)$$

where V_{Ref} = voltage observed on the reference component, and

V_{Mast} = voltage observed on the master record

The continuous background spectrum represents antenna noise.

All the AM radio transmitters are vertical electric dipoles, so oriented to take advantage of the preferred TM mode of propagation. Thus it is not surprising that the dominant component observed is horizontal. Since the AM stations are to the north and south of Richmond, the E-W component is generally larger than the N-S component. The station at 55.5 kHz shows the E-W component slightly stronger than the N-S one, consistent with the northeast or southwest direction indicated by Figure 4b. Several signals noted on one horizontal component at frequencies between 10 and 100 kHz are not distinguishable in the other component. While this could indicate that they are due to stations located precisely along a cardinal direction from the field location, it is actually because the respective transmitters weren't keyed on during the data run (as was verified visually by observing the spectrum).

Comparisons between the two EMCO coils using ambient fields

The two EMCO coils were arranged in parallel in a general east-west direction so as to observe the primary components of the AM radio stations. Simultaneous data were collected, first with EMCO antenna "A" connected to Channel 1 of the HP89410 and "B" to Channel 2 (case I), and then with the antennas interchanged on the ends of the cables (case II). We can deduce the different sensitivities and phase responses from this procedure by considering each indicated response to be of the form

$$V_{obs} = C_{AorB} * k_{1or2} \tag{23}$$

where C is the sensitivity of the coil, and

k is the response function of the cable and channel

Taking ratios and differences to isolate the amplitudes and phases of the sensitivity functions, we find that

$$C_B / C_A = \sqrt{\frac{V_{AII} / V_{BII}}{V_{AI} / V_{BI}}} \tag{24}$$

and $$\Delta\phi = \frac{\Delta\phi_{AI} + \Delta\phi_{BII}}{2} \qquad (25)$$

Table III shows the amplitude differences, in percent, and the phase differences, in degrees, between the responses of the two antennas.

Table III: Comparison of EMCO antenna response functions

freq, kHz	Del Sensitivity, %	Del Phi, deg
560	-3.6	-1.4
610	-0.9	-1.9
680	0.0	-1.4
740	-0.4	-1.1
810	-0.6	-0.9
910	-0.4	-0.6
960	0.1	-0.9
1010	-0.5	-1.0
1050	-0.5	-0.8
1100	-1.6	-0.3
1220	1.1	0.2
1260	0.1	-1.4
1310	3.2	(n.d.)
1400	-0.3	-0.4
1450	2.2	1.2
1550	0.0	-1.2
Averages:	-0.13	-0.81
RMS:	1.5	1.1

These results show that the two antenna amplitude responses are within about 1½% of each other, and the phases are within one degree, and better on the average.

Attitude and Ellipse Results

The attitude of the polarization plane and the ellipse parameters were calculated by the methods outlined above. Table IV presents the direction cosines of the normals to the

planes of polarization and the in-plane tilt and ellipticities, in percent, for each of the AM broadcast stations listed in Table II.

Table IV: Plane of Polarization and Ellipse Parameters

Freq	Nx-hat	Ny-hat	Nz-hat	Tilt,deg	Ellip,%
560	0.141	0.018	-0.990	0.2	-3.6
610	-0.046	-0.023	0.999	-0.1	-7.7
680	-0.056	-0.023	0.998	0.0	-7.6
740	0.016	0.029	-0.999	0.0	-6.2
810	-0.053	0.020	-0.998	0.2	-6.5
910	0.060	0.015	-0.998	-0.3	-3.8
960	0.048	-0.016	0.999	0.6	-10.8
1010	0.000	0.017	-1.000	0.1	-3.4
1050	-0.175	-0.028	0.984	0.0	-3.9
1100	-0.009	-0.027	1.000	-0.4	-9.7
1220	-0.291	0.010	-0.957	0.1	-2.3
1260	0.047	-0.005	0.999	0.2	-6.5
1310	-0.119	-0.028	0.993	-0.6	-6.8
1400	-0.342	0.067	-0.937	-0.2	-2.6
1450	-0.287	-0.015	-0.958	0.0	-0.9
1550	-0.086	0.024	-0.996	-0.2	-2.9

We note that the polarization planes are nearly flat-lying, as evidenced by the dominantly vertical normals. The broadcast signals are directed within a degree of the line-of-sight bearing to their respective transmitters, as indicated by the tilt angles, which show the deviation from the *x*-axis or line-of-sight when the polarization plane lies horizontal. Furthermore, the AM broadcast signals are very nearly linearly polarized, as demonstrated by the generally low ellipticities. Station KFAX at 1100 kHz was observed to have a large frequency drift, changing by almost 1.0 Hertz per minute; this trait rendered accurate determinations of the signal inaccurate, leading to the relatively large ellipticity shown in Table IV. No explanation has been found for the large ellipticity of KABL at 960 kHz.

Conclusions

Based on these data, we conclude that it is reasonable to make high-frequency magnetic field measurements at least to frequencies of about 1 MHz using the EMCO Model 6507 coils as sensors. Further, we note that the magnetic component of the AM radio station fields at Richmond Field Station is only very weakly elliptically polarized in nearly horizontal planes.

Acknowledgement

This work was carried out under U.S. Department of Energy Contract DE-AC03-76SF-00098. Funding was provided by the U.S. Department of Energy, the Environmental Management Sciences Program, as EMSP Project No. 60328.

References

Bak, N.H, Sternberg, B.K., Dvorak, S.L., and Thomas, S.J., 1993, Rapid high-accuracy electromagnetic soundings using a novel four-axis coil to measure magnetic field ellipticity, Jour. App. Geophys, vol. 30, pp.234-245

Beckman, P., 1968, The depolarization of electromagnetic waves, Golem Press, Boulder, Colorado

Booker, H.G., Rumsey, V.H., Deschamps, G.A., Kales, K.L., Bohnert, J.I., 1951, Techniques for handling elliptically polarized waves with special reference to antennas, Proc. I.R.E., vol. 39, pp.533-552

Born, M., and Wolf, E., 1970, Principles of optics, Pergamon Press, Oxford

Burrington, R.S., 1933, Handbook of mathematical tables and formulas, Handbook Publishers, Sandusky, Ohio

Deschamps, G.A., and Mast, P.E., 1973, Poincare sphere representation of partially polarized fields, IEEE Trans. Ant. & Prop., vol. AP-21, no. 4 (July)

Halliday, D., and Resnick, R., 1960, Physics for students of science and engineering, John Wiley & Sons, New York

IEEE, 1983, IEEE Standard 145-1983: Standard definitions of terms for antennas, IEEE Trans Ant. & Prop., vol. AP-31, Part 2 (Nov)

Kraus, J.D., 1982, Radio astronomy, Cygnus-Quasar Books, Powell, Ohio

MacNeill, J.D., and Labson, V.F., 1991, Geological mapping using VLF radio fields *in* Electromagnetic methods in applied geophysics, M.N. Nabighian, *Editor*, Investigations in Geophysics series, No. 3; S.E.G., Tulsa

Morgan, M.G., and Evans, W.G., 1951, Synthesis and analysis of elliptic polarization loci in terms of space-quadrature sinusoidal components, Proc. I.R.E., vol. 39, pp. 552-556

Nichols, E., Morrison, H.F., and Clarke, J., 1988, Signals and noise in measurements of low-frequency geomagnetic fields, JGR, vol. 93, no. B11, (November 10)

Smith, B.D., and Ward, S.H., 1974, On the computation of polarization ellipse parameters, Geophysics, vol. 39, no. 6 (Dec.)

Stutzman, W.L., 1993, Polarization in Electromagnetic Systems; Artech House, ISBN 0-89006-508-X

Theocaris, P.S., 1979, Elliptic polarization represented by the Carter and Smith charts, Applied Optics, vol. 18, no. 23 (Dec)

Thomas, S.J., 1996, Modeling and testing the LASI electromagnetic subsurface imaging system; Ph.D. dissertation, Univ. of Ariz., Tucson

Appendix I: Interpolated Calibrations for the EMCO Model 6507 Magnetic Loop Antennae

Figures AI -1, -2, and -3 present the interpolated calibration data for the EMCO Model 6507 in useful alternative forms of sensitivity, in μA/m/volt, antenna factor, in dB((μA/m)/volt), and effective area, in m^2.

Figure 1:
Solenoid Calibration

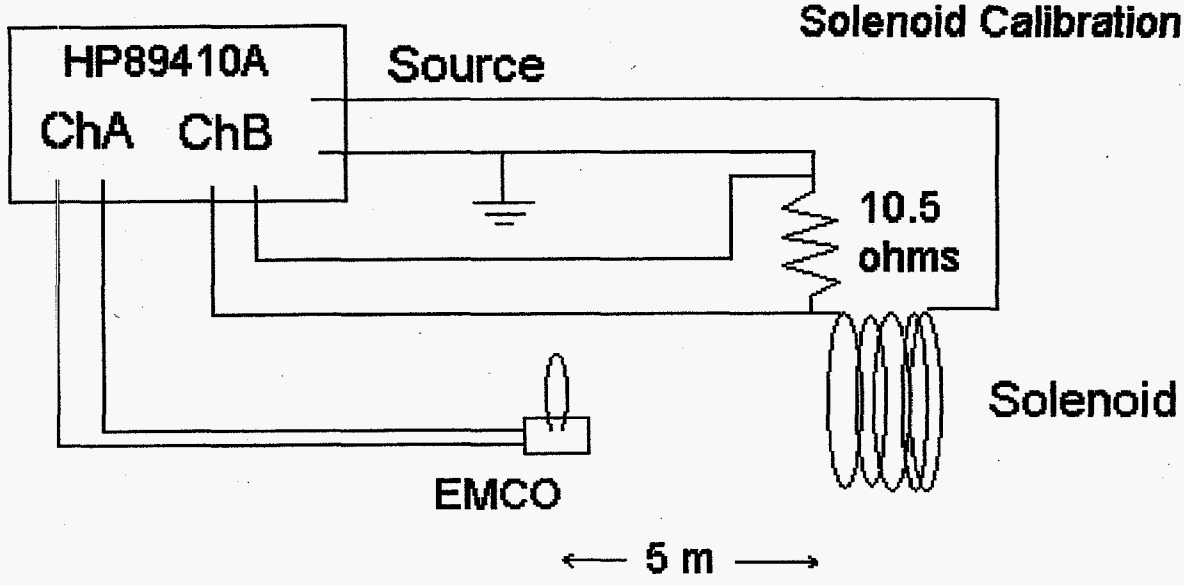

Fixed-source calibration setup
for EMCO 6507 coil

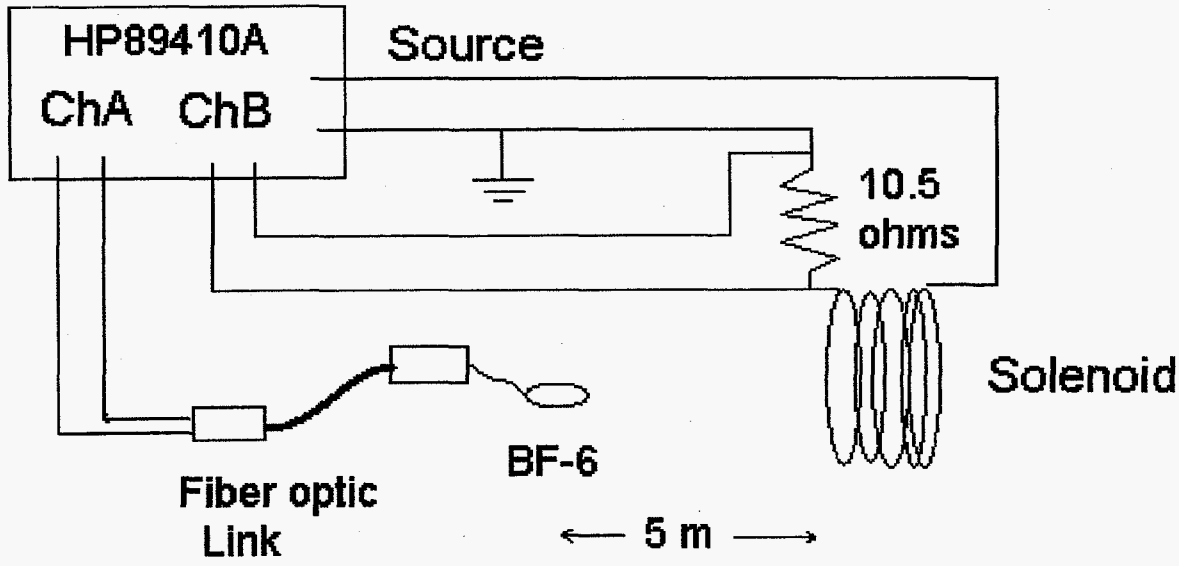

Fixed-source calibration setup
for BF-6 coil, showing optical link

Figure 2:
Solenoid calibration of BF-6 s/n 9506

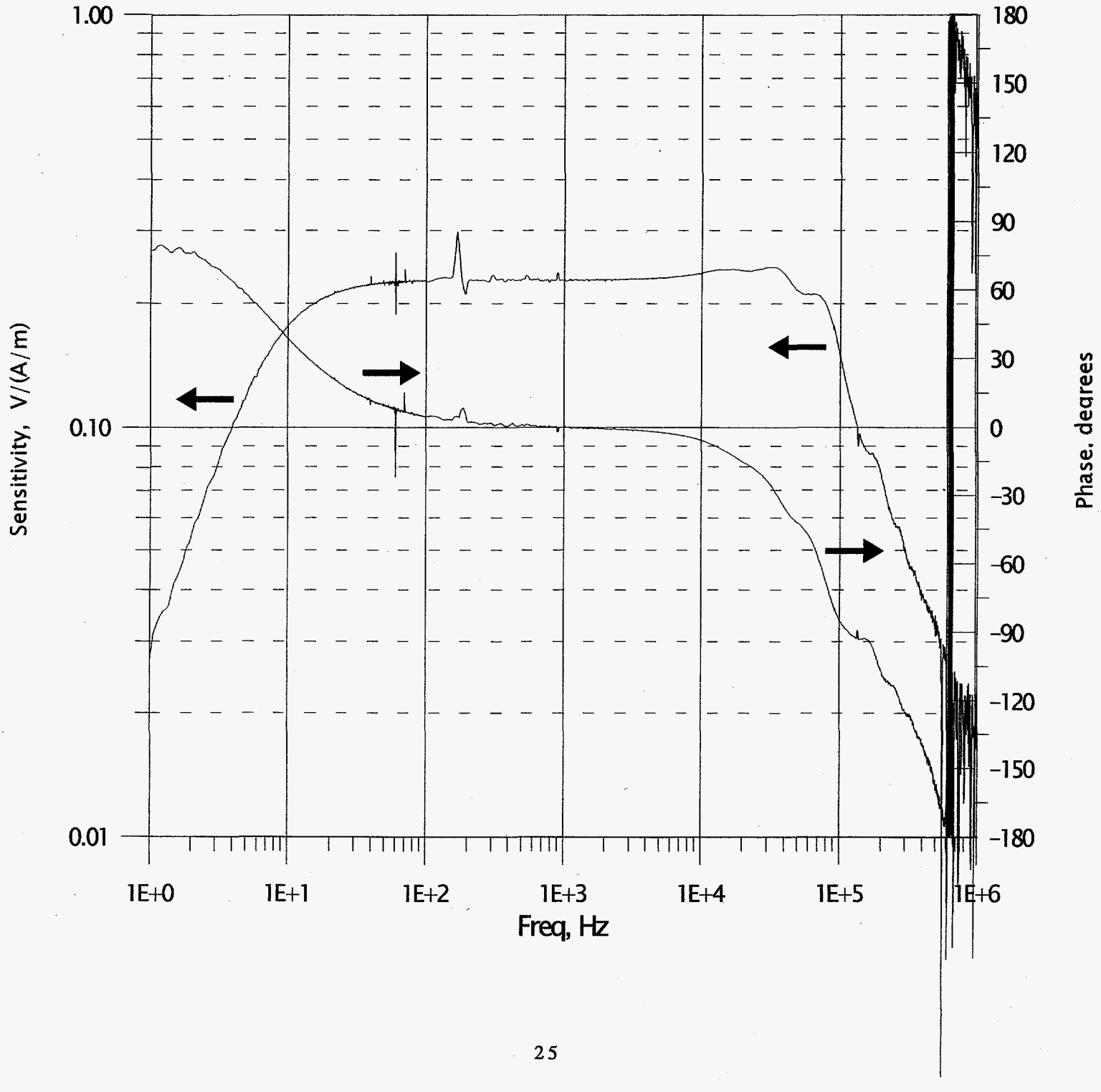

Figure 3:
EMCO Model 6507 Calibration

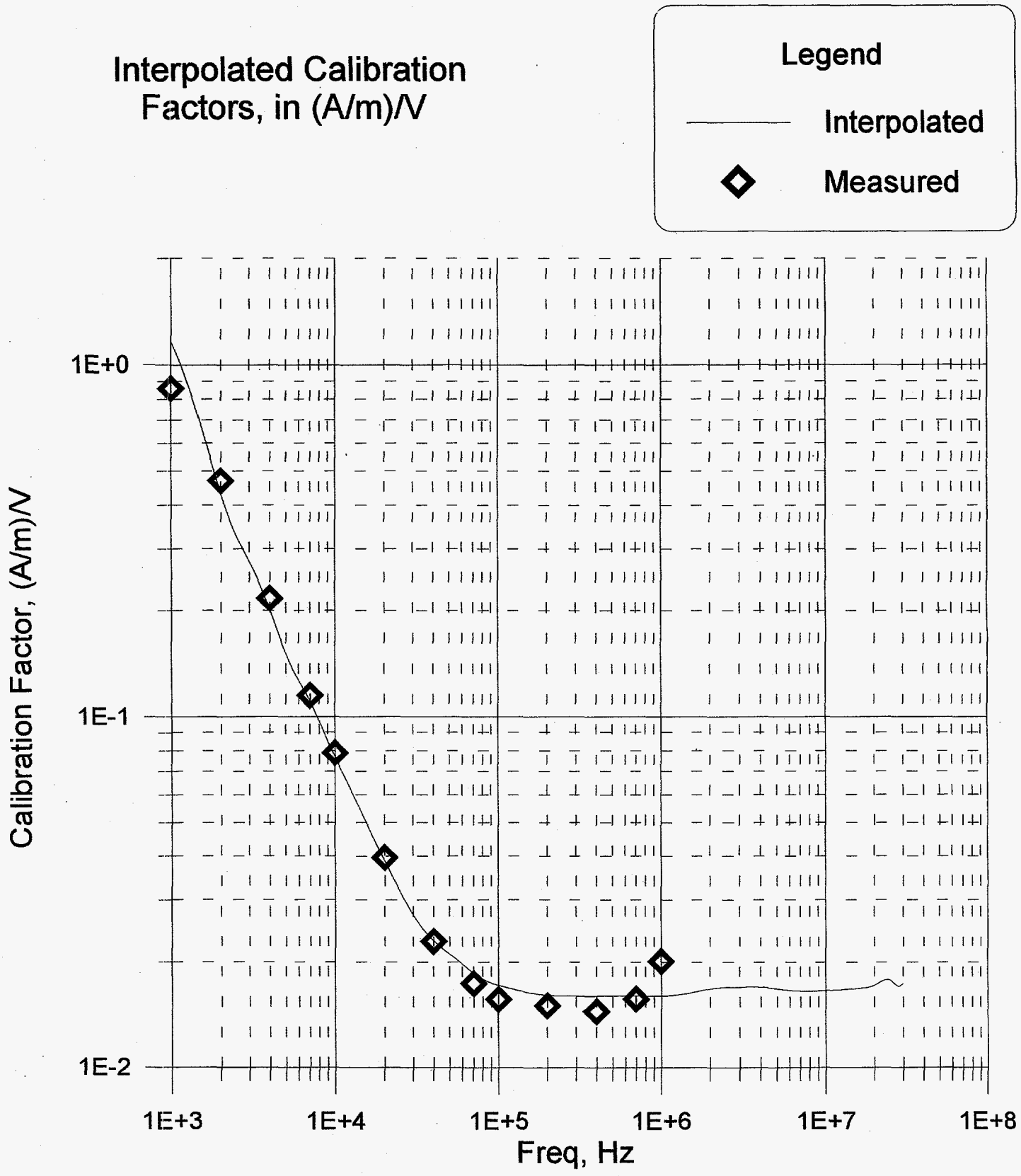

Figure 4a:
EMCO angular response at 910 kHz

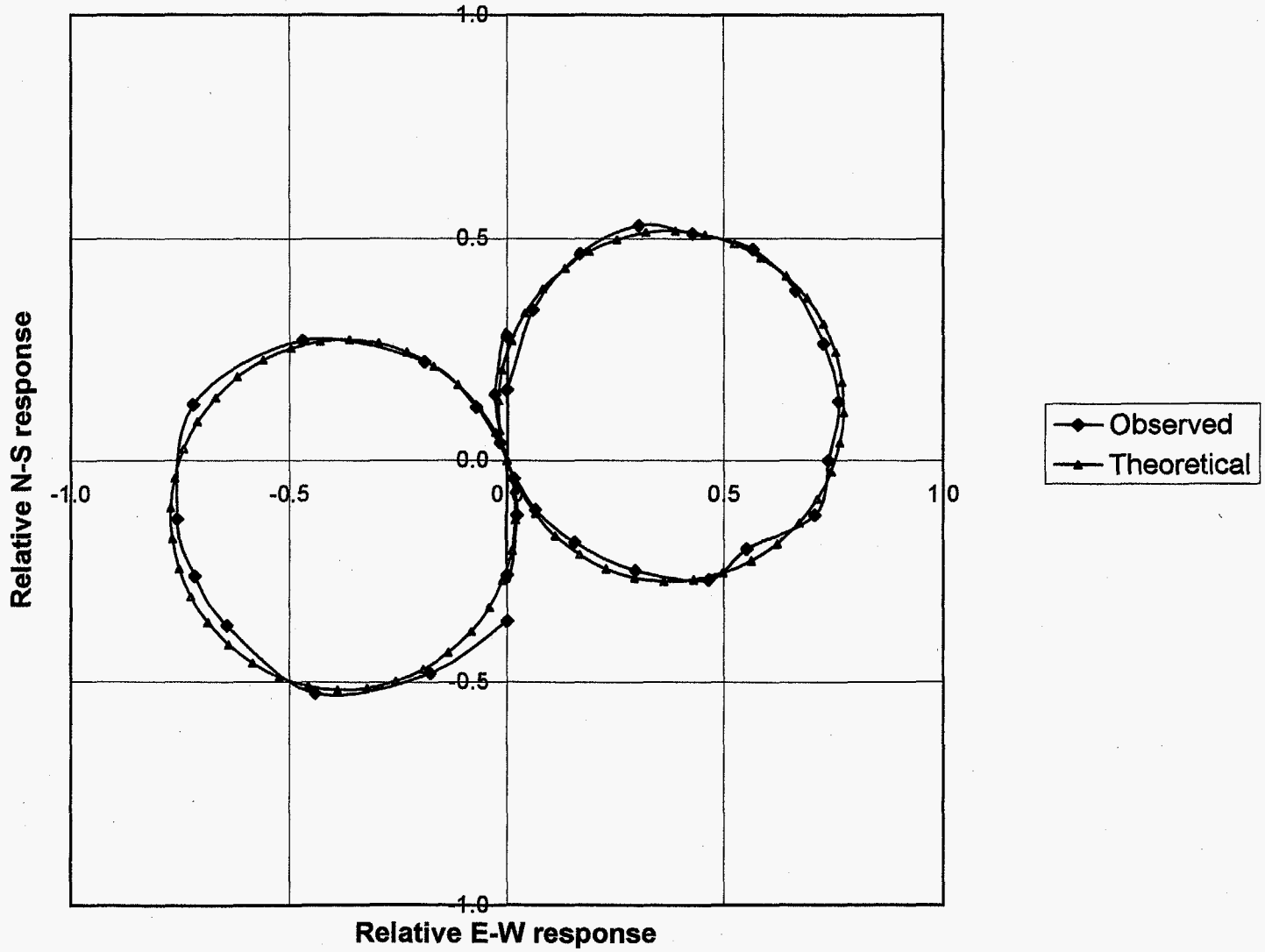

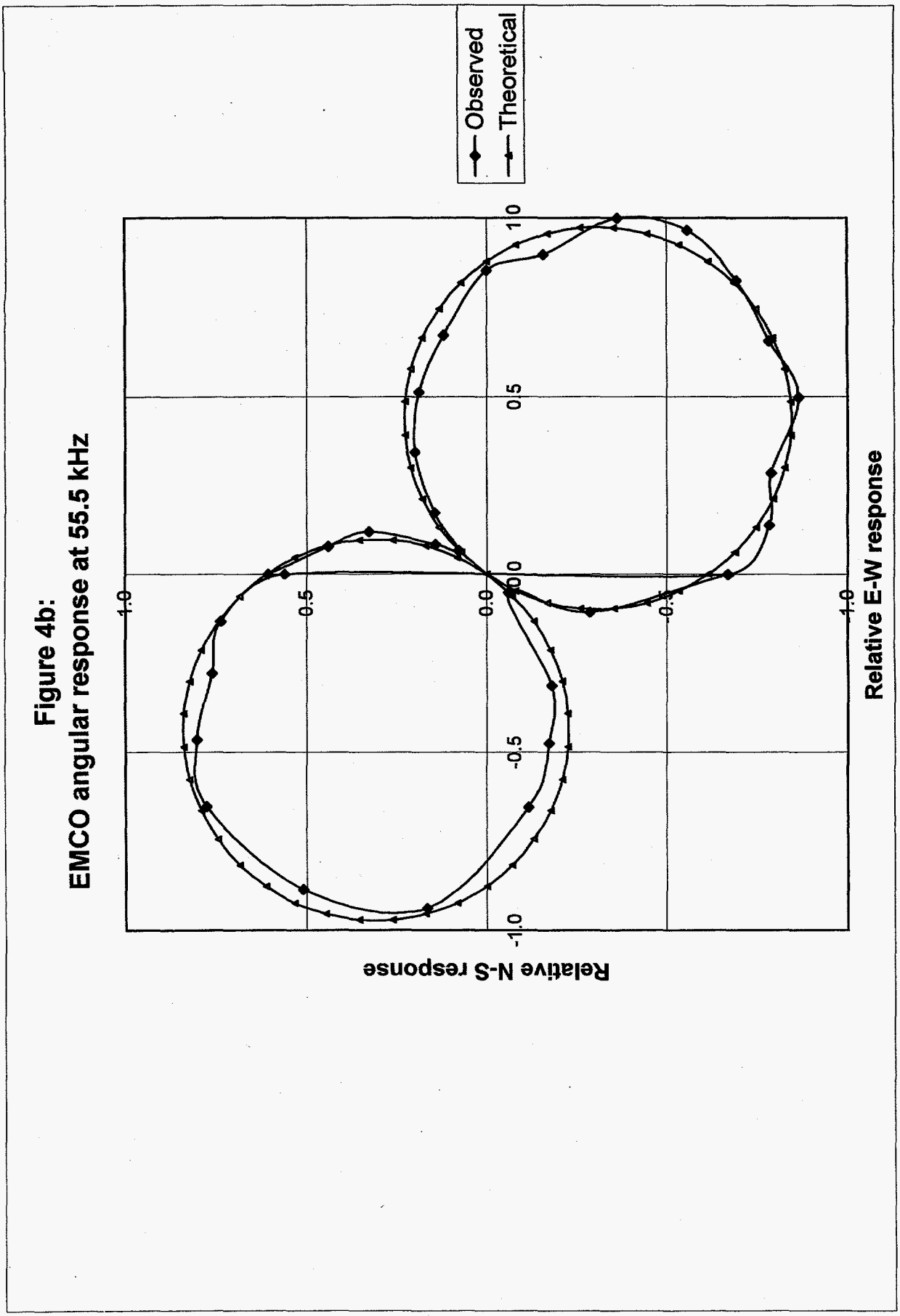

Figure 4b:
EMCO angular response at 55.5 kHz

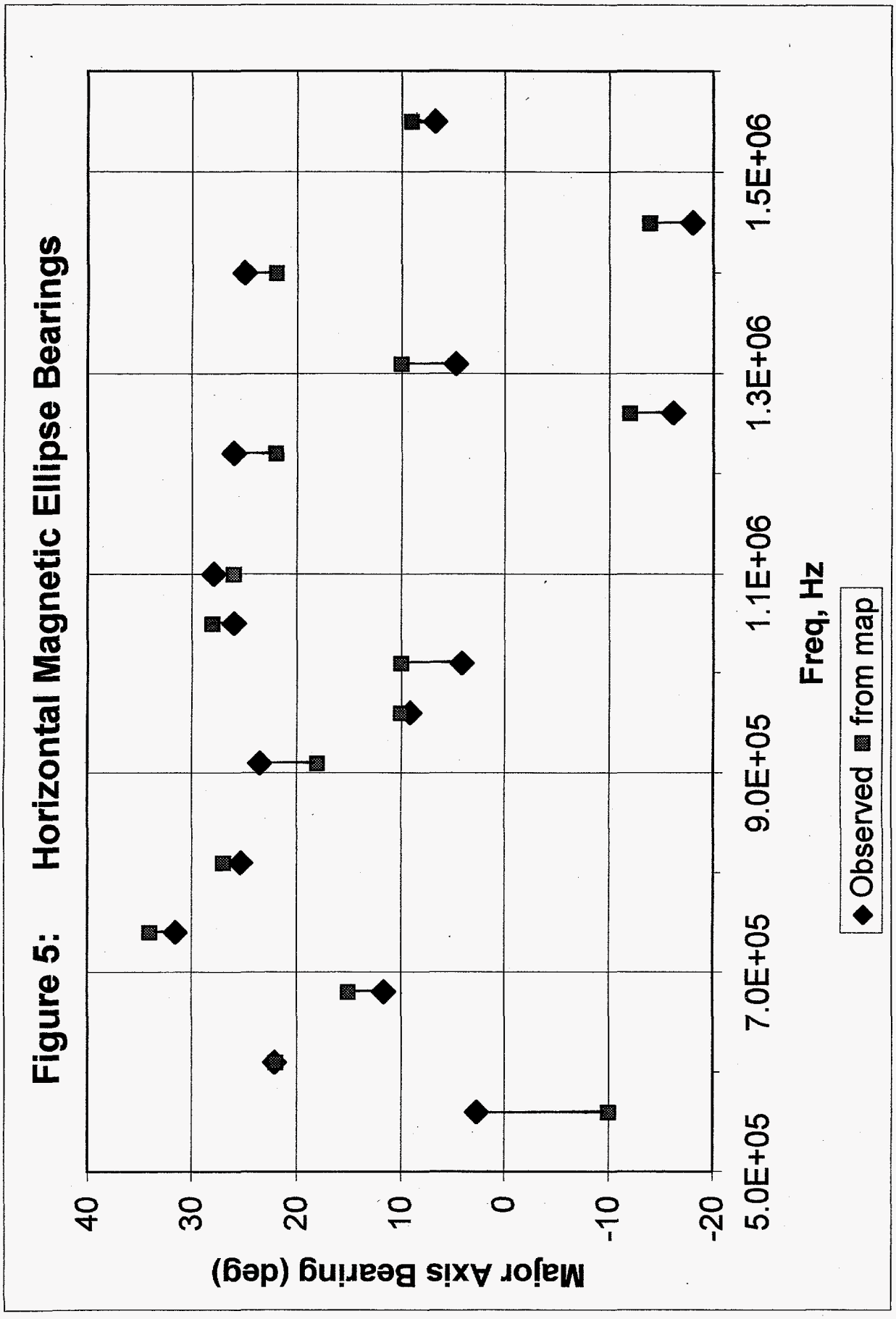
Figure 5: Horizontal Magnetic Ellipse Bearings
Major Axis Bearing (deg)
40
30
20
10
0
-10
-20
5.0E+05
7.0E+05
9.0E+05
1.1E+06
1.3E+06
1.5E+06
Freq, Hz
◆ Observed ■ from map

Figure 6:
EMCO coil Noise
expressed as equivalent
magnetic field, (A/m)/sqrt(Hz)

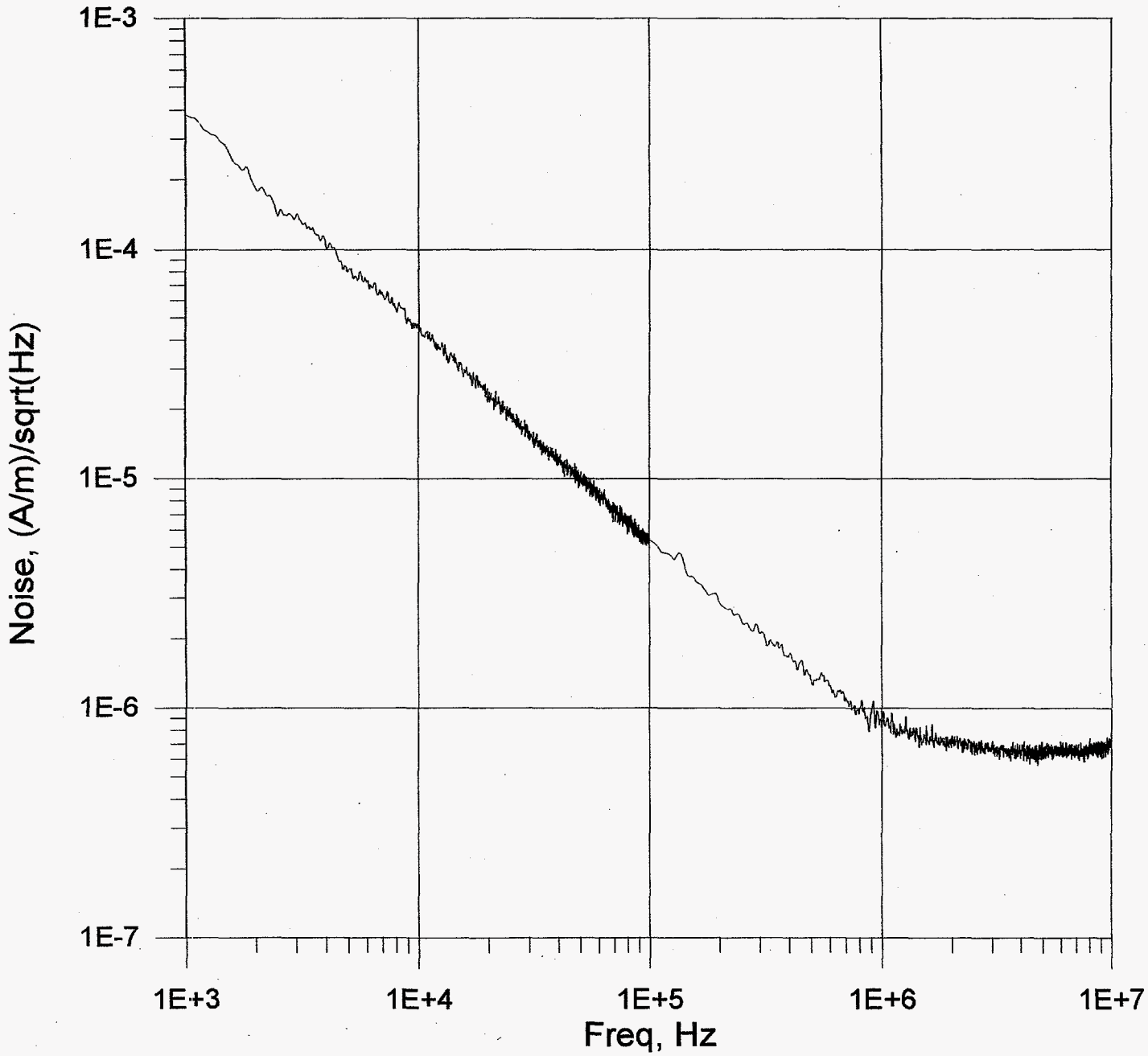

Figure 7:
Detailed view of KNEW (910 kHz) spectrum

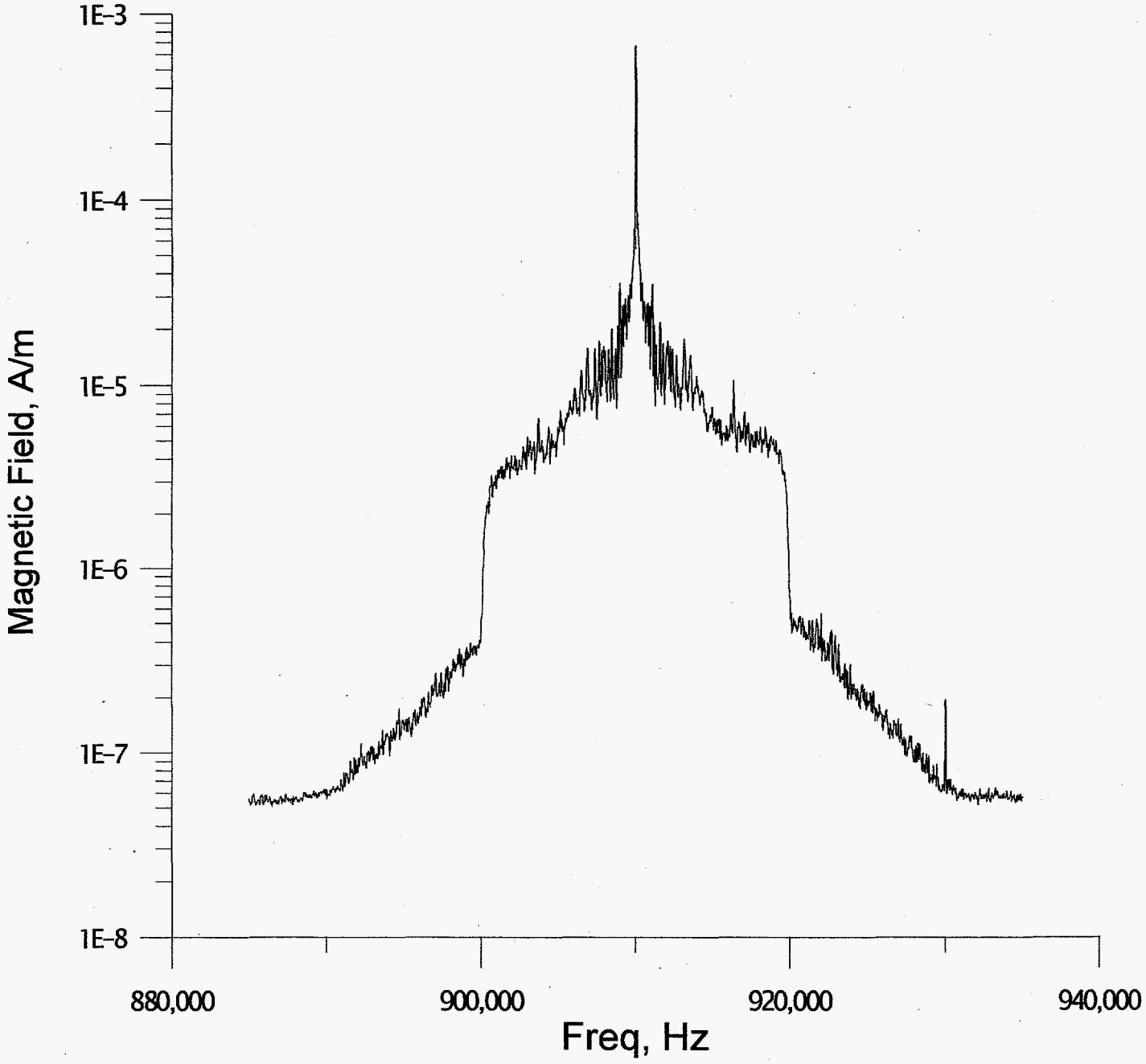

Figure 8:
Typical Ambient Field at Richmond Field Station

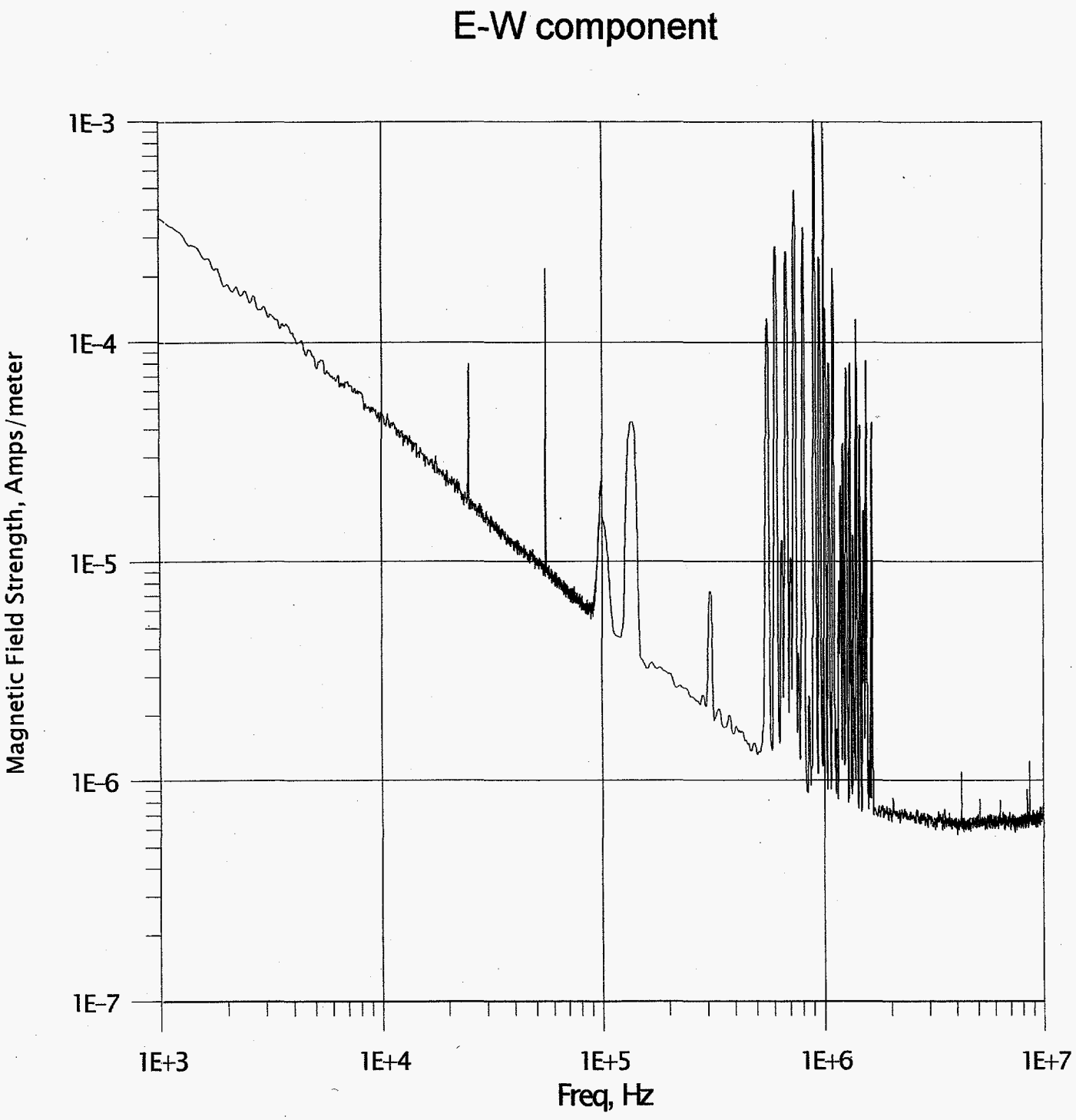

Figure 9:
Typical Ambient Field at Richmond Field Station

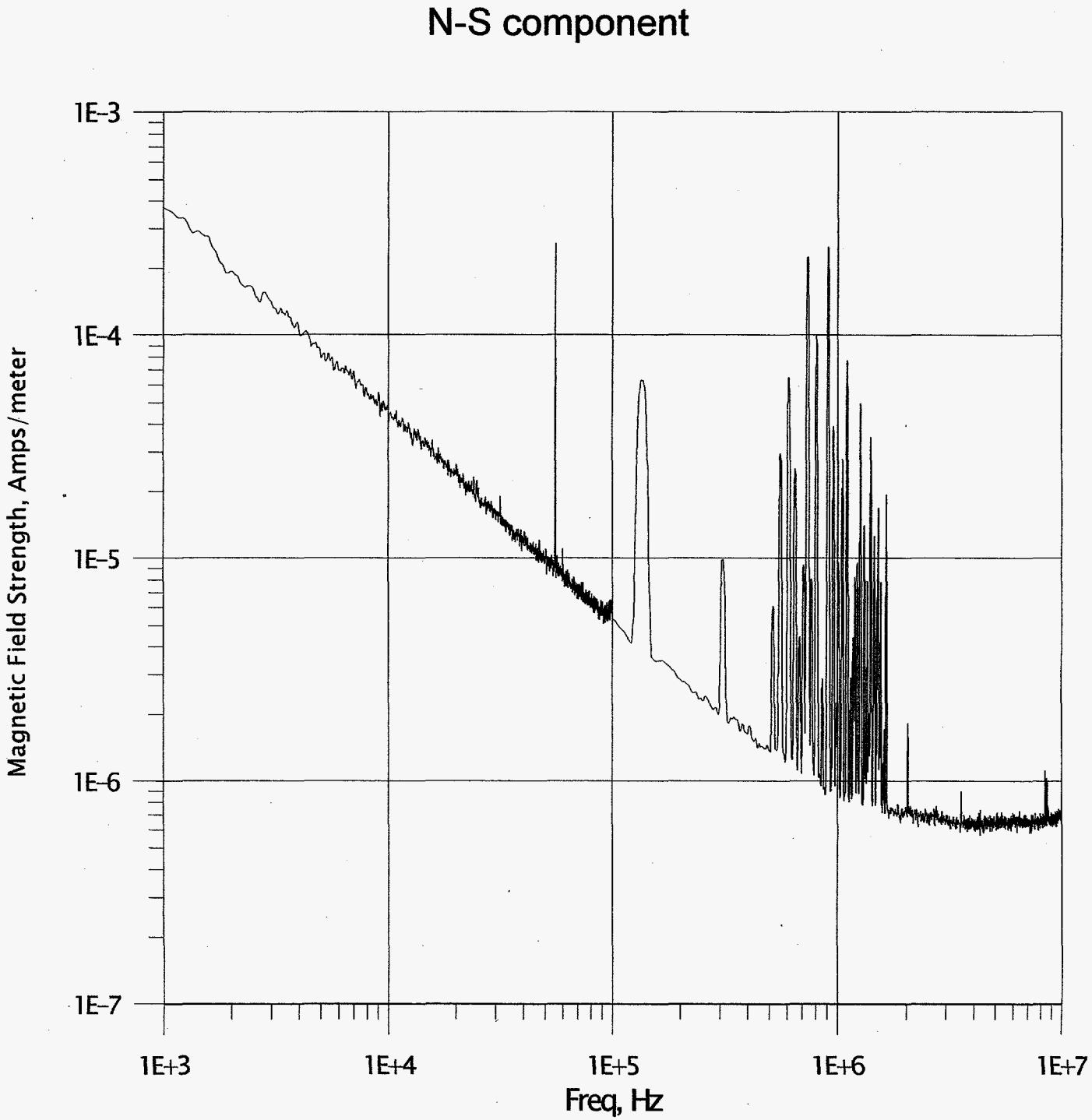

Figure 10:
Typical Ambient Field at Richmond Field Station

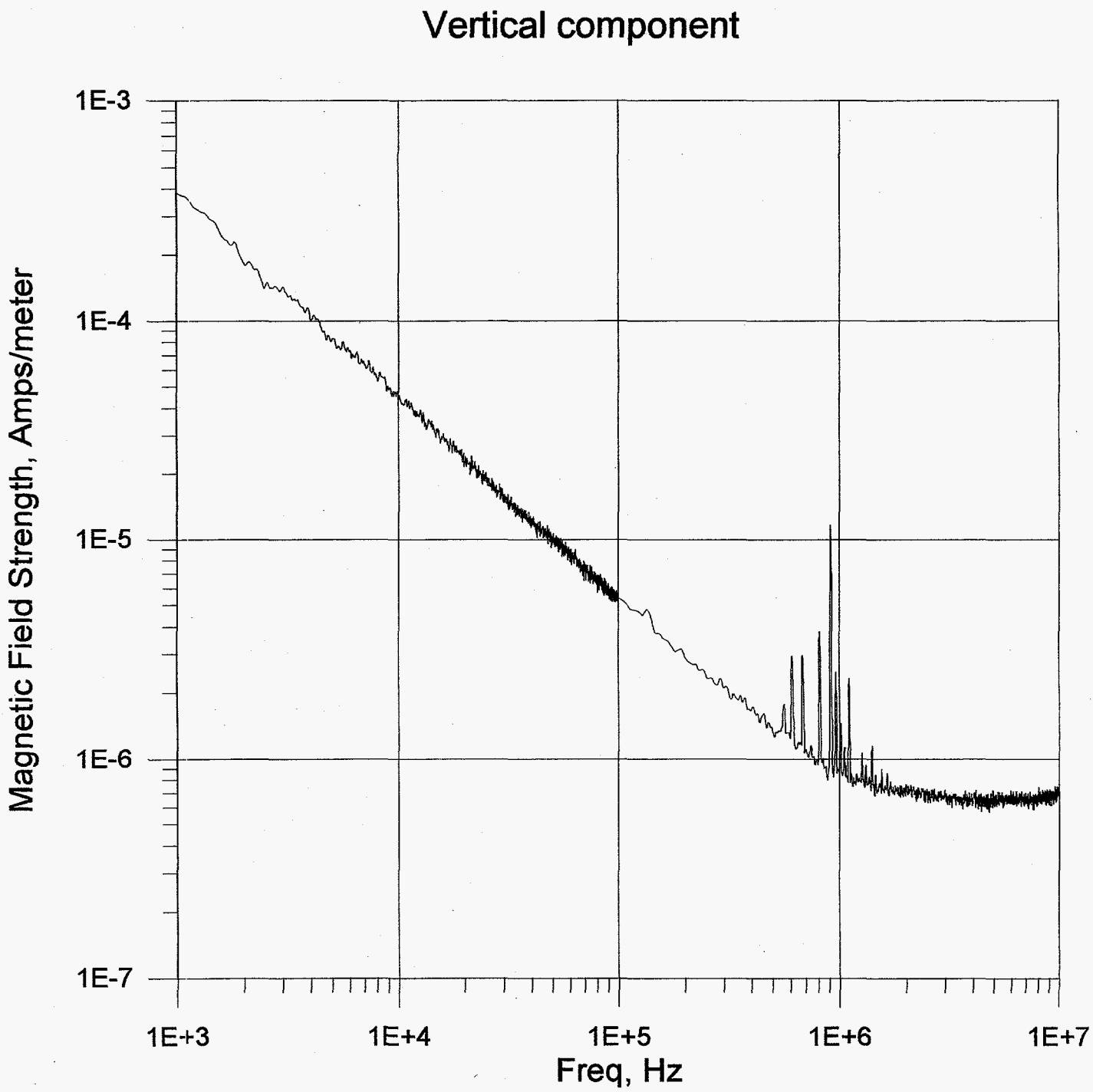

Appendix I: Interpolated Calibrations for the EMCO Model 6507 Magnetic Loop Antennae

Figures AI -1, -2, and -3 present the interpolated calibration data for the EMCO Model 6507 in useful alternative forms of sensitivity, in μA/m/volt, antenna factor, in dB((μA/m)/volt), and effective area, in m^2.

Figure A1-1:
EMCO Model 6507 Calibration

Interpolated Sensitivity, in V/(A/m)

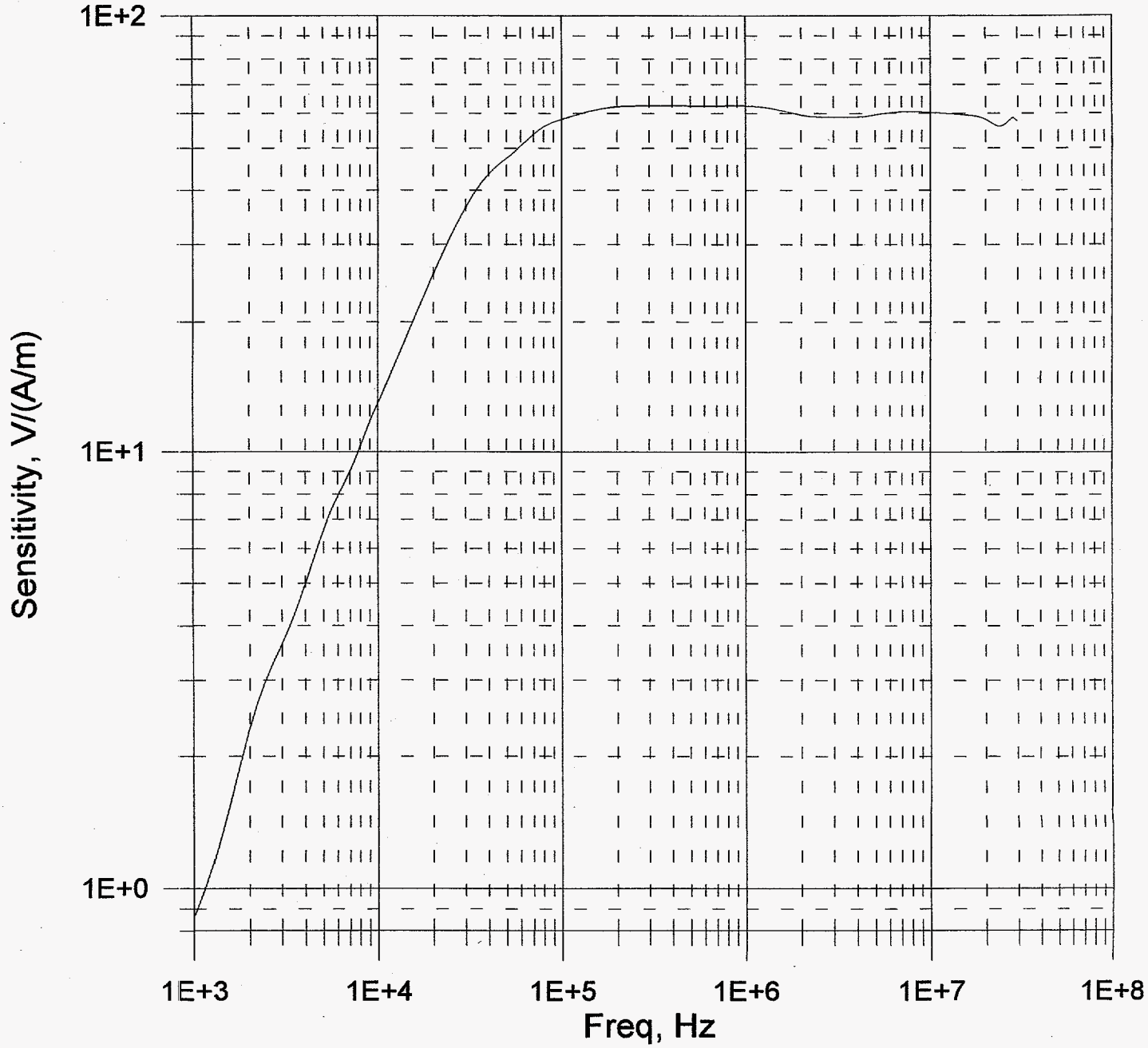

Figure A1-2:
EMCO Model 6507 Calibration

Interpolated Antenna Factors, AF, in dB

AF = 20 * log (A/m)/V

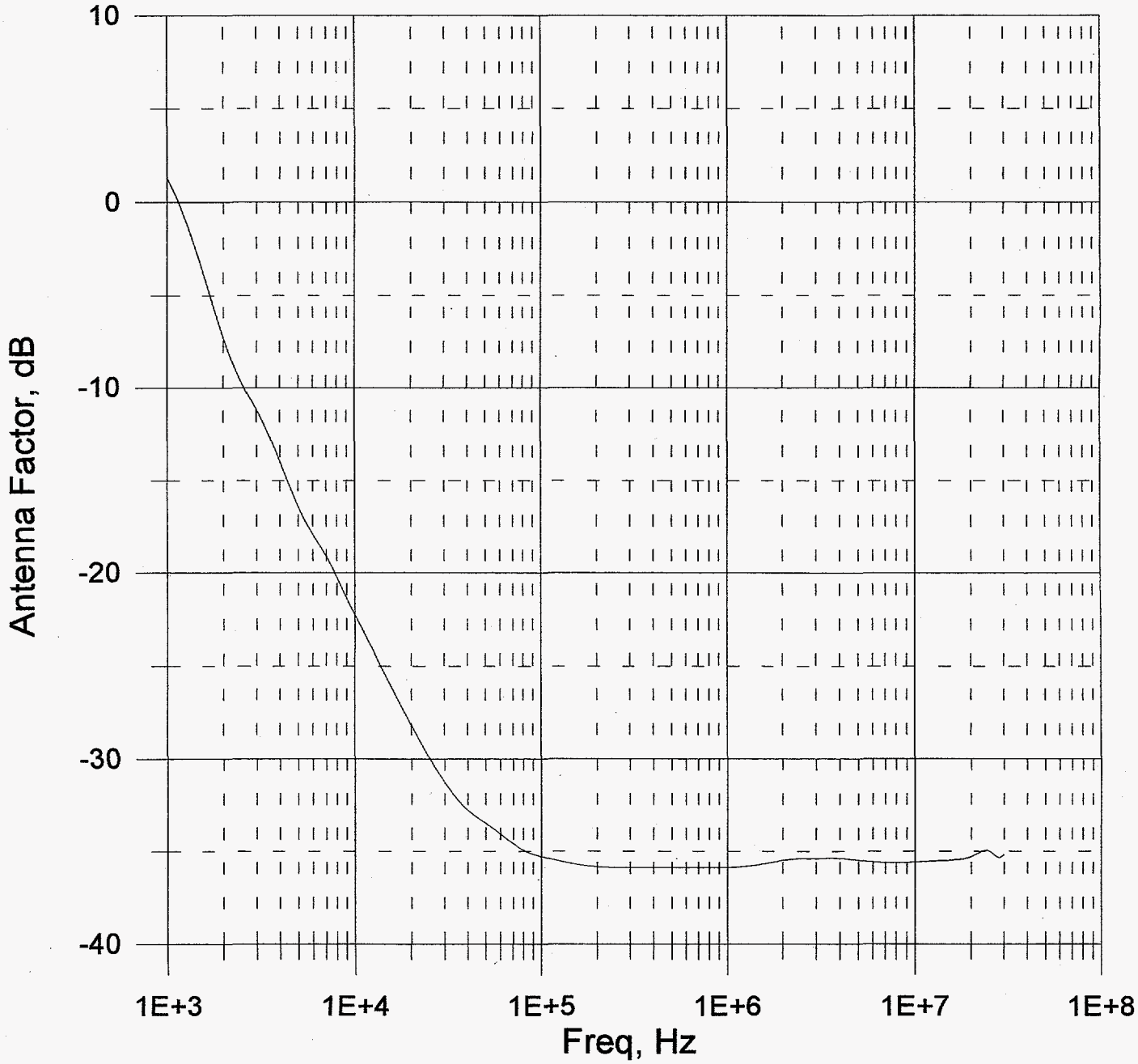

Figure A1-3:
EMCO Model 6507 Calibration

Interpolated Effective Area, in square meters